THE STRUCTURE OF JAHN-TELLER POLARONS IN THE COLOSSAL MAGNETORESISTIVE MANGANITES

B. J. Campbell, S. J. L. Billinge, J. W. Lynn, R. Osborn and S. K. Sinha*

I. INTRODUCTION

The observation of large negative magnetoresistive effects[1,2,3] has generated tremendous scientific and technical interest in the perovskite manganites and related materials. These phenomena are commonly classified under the heading "colossal magnetoresistance" (CMR) to distinguish them from magnetoresistive effects in metals and metal-multilayers. CMR effects are observed in conjunction with the formation of a ferromagnetic metallic (FM) state at low temperatures and/or high magnetic fields. The close connection between the magnetism and the charge transport in these mixed-valence Mn^{3+}/Mn^{4+} materials is commonly believed to have its origin in the magnetic double-exchange interaction[4,5], in which itinerant e_g electrons mediate the ferromagnetic coupling between neighboring Mn core spins. Recent works have shown that double-exchange alone is insufficient to explain the extraordinary magnetoresistance values observed experimentally, so that electron-phonon interactions must also be invoked.[6,7] Alternatively, a direct Mn-Mn magnetic exchange interaction has been reported to better explain[8] the insensitivity of the Curie temperature (T_C) to the carrier concentration in oxygen-depleted samples.[9] This model also relies on strong electron-lattice coupling, which occurs via the Jahn-Teller (JT) mechanism[10], in which an $Mn^{3+}O_6$ octahedron experiences a spontaneous distortion designed to break the degeneracy of its e_g orbital, and thus lower the energy of its extra electron. If the coupling is strong, the electron may

* Branton J. Campbell, Materials Science Division, Argonne National Laboratory, Argonne IL 60439. S.J.L. Billinge, Department of Physics and Astronomy, Michigan State University, Lansing, MI 48824. Jeffrey W. Lynn, NIST Center for Neutron Research, National Institute of Standards and Technology, Gaithersburg, MD 20899 and University of Maryland, College Park, MD 20742. Ray Osborn, Materials Science Division, Argonne National Laboratory, Argonne IL 60439. Sunil K. Sinha, Physics Department, University of California, San Diego, CA 92093.

induce a significant local distortion of the lattice, which then follows the electron as it hops from site to site, thus forming a polaron.[8,11,12]

Coherent JT distortions, which indicate a long-range ordering of the occupied e_g orbital configuration, occur in purely Mn^{3+} systems such as $LaMnO_3$, as well as in charge-ordered systems like $La_{0.5}Ca_{0.5}MnO_3$.[13] The incoherent or local distortions associated with hopping JT polarons are also considered to be an important structural feature of the perovskite manganites. This has been amply verified as a wealth of evidence now shows the formation and collapse of the polaronic state to be essential to the large magnetoresistance that accompanies the transition to the FM state, and demonstrates that the spin, charge, orbital, and lattice degrees of freedom are all intimately coupled. JT polarons have been studied in the manganites using a variety of experimental techniques that includes a number of spectroscopies (e.g. UV/IR, Raman, NMR, EPR, μSR, inelastic neutron scattering, XAFS, etc.), thermodynamic and transport measurements (optical conductivity, resistivity, magnetoresistance, Hall effect, thermopower, thermal expansion, etc.), as well as dilatometry, and scanning probe microscopy. Broad summaries of these findings have been given elsewhere.[14]

This article considers the structural characterization of JT polarons, primarily reviewing our use of x-ray and neutron scattering to probe polaronic local structure. Section II of this article considers the coherent JT distortions associated with such long-range charge and/or orbital order. Sections III-V then focus on the incoherent JT distortions associated with the local polaronic structure. Section III discusses deviations from crystallinity and the methods of local structure analysis; section IV reviews the contributions of the PDF and Rietveld methods; section V describes the measurement and importance of polaron-induced lattice strain fields; and finally, section VI reviews short-range polaron correlations.

II. CHARGE AND ORBITAL ORDER IN THE MANGANITES

Early diffraction experiments on the manganite perovskites demonstrated that the MnO_6 octahedra in a number of manganite perovskites experience JT distortions in addition to octahedral rotations. Rotations about pseudo-cubic (100) axes can occur in response to an A-site cation slightly smaller than the corresponding interstitial volume, and tend to yield orthorhombic lattice parameters ($a \sim \sqrt{2}a_{cub}$, $b \sim \sqrt{2}a_{cub}$, $c \sim 2a_{cub}$) such that $c/(\sqrt{2}a) > 1$ (the so-called "O" phase). Cooperative JT distortions appear in some systems, such as $LaMnO_3$, and produce a distinct orthorhombic phase (O´) that usually obeys the condition, $c/(\sqrt{2}a) < 1$, with no additional cell-doubling beyond that dictated by the octahedral tilts. In the O´ phase, each $Mn^{3+}O_6$ octahedron experiences an apical stretch, making one of its three Mn-O bonds longer than the other two by as much as 0.25 Å.[15] The distortions cooperate to minimize the resulting elastic-strain energy so that all of the long bonds lie in the orthorhombic *a-c* plane and form a checkerboard-like pattern of perpendicular in-plane distortion directions as seen in Fig. 1. An early review by Goodenough[16] contains an unusually detailed catalogue of perovskite structures and properties.

A classic series of neutron powder diffraction experiments[17] on $La_{1-x}Ca_xMnO_3$ in the mid-1950's uncovered a wide array of distinct magnetic orderings, that were successfully explained by J. B. Goodenough in terms of ordered sublattices of Mn^{3+} and Mn^{4+} charges together with cooperative JT distortions on the Mn^{3+} sublattice.[13] In addition to corroborating the observed magnetic orderings, these hypothetical charge and orbital

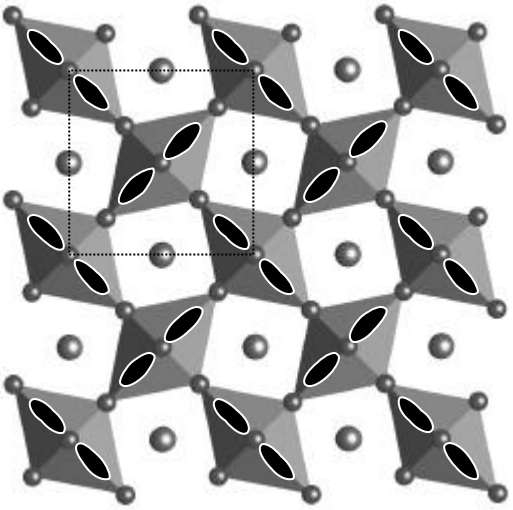

Figure 1. Illustration of the cooperative JT distortions and the in ferred orbital ordering in the 100% Mn^{3+} lattice of $LaMnO_3$. These idealized distortions involve a primary apical stretch of one of the Mn-O bond pairs. After figure 4 of Goodenough.[12] Pairs of ovals indicate occupied e_g orbitals.

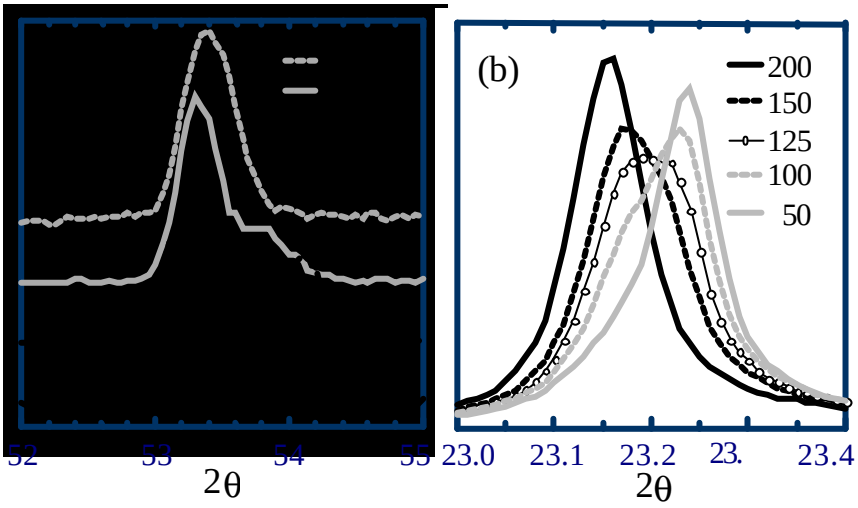

Figure 2. (a) A second-phase (0,3,1) reflection tracks the development of the low-temperature C/O-ordered phase in $La_{0.5}Ca_{0.5}MnO_3$. The peak on the left contains the (0,3,1) of the primary high-temperature phase as well as the unresolved (2,1,1) and (1,1,2) reflections. After Huang *et al.*[20] (b) The evolution of the (0,0,10) reflection through the C/O-AF transition in $LaSr_2Mn_2O_7$. The peak on the left corresponds to the high-temperature phase which develops C/O order at $T_{CO} \sim 210$K. The peak on the right, corresponding to the competing A-type AF phase, appears as a shoulder at $T_N = 170$ K and largely consumes the C/O-ordered phase by 100 K. After Argyriou *et al.*[25]

ordering patterns also provided qualitative predictions for ordering temperatures, lattice parameters, and magnetic sublattice moments that agreed well with observations. However, a charge-ordered sublattice multiplies the unit cell size and also predicts the appearance of non-magnetic superlattice reflections, which were not observed at that time.

The observation of these super-structural signatures has only recently become possible with the development of bright high-resolution x-ray and neutron sources and modern electron diffraction instruments. In $La_{0.5}Ca_{0.5}MnO_3$, for example, which is ferromagnetic above T_C~260K and CE-type antiferromagnetic below T_N~160K, the appearance of weak superstructure reflections has been reported to develop between T_C and T_N.[18,19] A recent neutron powder diffraction (NPD) study shows this superstructure to appear at 230K as a second phase, in competition with the ferromagnetic phase[20], and subsequently hosts CE-type AF order below T_N. A careful Rietveld analysis of the superlattice peak intensities[19], using synchrotron x-ray powder diffraction (PXD) data, confirms Goodenough's earlier hypothesis of long-range charge/orbital (C/O) order, and the resulting zig-zag pattern of JT distortions is now commonly referred to as "CE-type" C/O order by association with CE-type magnetic order. Fig. 2a shows the appearance of a 2nd-phase (0,3,1) reflection to the right of the primary-phase (0,3,1) reflection that tracks the development of the C/O order. This peak arises because the lattice parameter perpendicular to the distortions, *b*, is significantly smaller in the JT-distorted region, whereas the lattice parameters in the *a-c* plane of the distortions grow larger. Long-range C/O order has now been observed in many manganite systems,[21,22] including some "charge-stripe" phases.[23,24]

A similar situation occurs in the bilayered $La_{1+2x}Sr_{2-2x}Mn_2O_7$ system. In $LaSr_2Mn_2O_7$ (x = 0.5), CE-type C/O order forms at T_{CO} ~ 210K, well above the AF ordering temperature.[25,26,27] Fig. 3 contains an illustration of this zig-zag orbital arrangement and the corresponding transverse displacements within a single perovskite sheet of this material. The oxygen displacements within the JT-distorted octahedra of this system are roughly 0.05 Å, which is about half that observed in $La_{0.5}Ca_{0.5}MnO_3$.[19] While the C/O-ordered phase of $LaSr_2Mn_2O_7$ has been reported to host CE-type AF order within a narrow temperature range[27], the predominant magnetic ordering in this material appears at T_N ~ 170K and consists of AF-coupled ferromagnetic sheets (i.e. A-type order). The A-type phase competes with the C/O-ordered phase until the C/O order is overcome below 100K. The (0,0,10) Bragg reflection, shown in Fig. 2b, has a low-angle component associated with the primary high-temperature phase that charge orders at T_{CO}. The right-hand shoulder is a 2nd-phase peak belonging to the A-type phase, which appears at T_N and grows with decreasing temperature until the C/O phase is consumed. The broad phase-coexistence regions seen in $La_{0.5}Ca_{0.5}MnO_3$ and $LaSr_2Mn_2O_7$ are typical of systems that exhibit C/O order. The local-disorder created by the solid-solution of size-mismatched A-site cations may create a microscopically inhomogeneous Jahn-Teller stabilization energy, though such an explanation needs more careful examination.

The $Pr_{0.7}Ca_{0.3}MnO_3$ system, which has a very small A-site cation-size mismatch, is interesting in that it exhibits a relatively sharp transition between a long-range C/O-ordered phase[28,29] and a low-temperature FM phase, accompanied by a very large CMR effect.[30] As the system is pushed from the C/O-ordered state into the FM metallic state by lowering the temperature, applying a magnetic field, or illuminating with an intense x-ray beam, the superstructure peaks diminish, indicating that the e_g electrons delocalize and the C/O order melts.[29,31] Generally, even in the absence of long-range C/O order, the competition between local JT distortions and ferromagnetic correlations persists and proves to be fundamental to CMR, as discussed below.

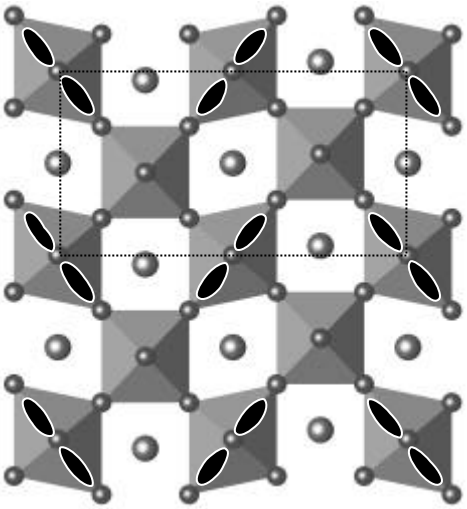

Figure 3. Illustration of charge-ordered sublattices and zig-zag (CE-type) charge and orbital order within a perovskite sheet of $LaSr_2Mn_2O_7$. After figure 4 of Goodenough.[12]

Because Mn^{3+} and Mn^{4+} have identical neutron cross-sections and nearly identical x-ray cross sections, neutron and x-ray diffraction are sensitive to orbital order rather than charge order. The superlattice reflections that we observe in C/O-ordered systems arise from the oxygen displacements induced by cooperative orbital order, while the charge-order is usually inferred. Polarized resonant x-ray diffraction techniques have now been applied to the CMR manganites for the purpose of obtaining independent measures of orbital and charge order.[32,33] Charge-ordered domains were shown to be many times larger than the orbitally ordered domains, both above and below T_{CO}, in the $Pr_{1-x}Ca_xMnO_3$ system (x = 0.4,0.5), demonstrating that the charge and orbital degrees of freedom are closely but not perfectly coupled.

III. LOCAL STRUCTURE FROM SCATTERING DATA

At specific compositions, such as undoped $LaMnO_3$, the JT polarons form a long-range ordered lattice. However, at general values of the composition the structure of JT polarons involves local deviations from perfect crystallinity. In the present context, the atomic displacements induced by the distortions are the deviations of interest. These displacements modify the diffracted intensities and give rise to diffusely-scattered intensity as well. Consider the effect of static local displacements on the elastic scattering distribution. This scattering is proportional to the structure function, which can be expressed as

$$I(\mathbf{Q}) = \left\langle \sum_{m,n} f_m e^{i\mathbf{Q}\cdot(\mathbf{r}_m+\mathbf{u}_m)} f_n^* e^{-i\mathbf{Q}\cdot(\mathbf{r}_n+\mathbf{u}_n)} \right\rangle = I_B(\mathbf{Q}) + I_D(\mathbf{Q}), \quad \text{where} \qquad (1)$$

$$I_B(\mathbf{Q}) = \sum_{m,n} (f_m d_m)(f_n^* d_n^*) e^{i\mathbf{Q}\cdot(\mathbf{r}_m - \mathbf{r}_n)}, \quad (2)$$

$$I_D(\mathbf{Q}) = \sum_{m,n} f_m f_n^* (d_{mn} - d_m d_n^*) e^{i\mathbf{Q}\cdot(\mathbf{r}_m - \mathbf{r}_n)}, \quad (3)$$

$$d_{mn} \equiv \left\langle e^{i\mathbf{Q}\cdot(\mathbf{u}_m - \mathbf{u}_n)} \right\rangle \text{ and } d_n \equiv \left\langle e^{i\mathbf{Q}\cdot\mathbf{u}_n} \right\rangle. \quad (4)$$

Here, the f_n are the x-ray or neutron scattering factors, while the $\mathbf{r}_n$, and $\mathbf{u}_n$ are the respective ideal atomic positions, and displacements from those ideal positions, summed over the whole crystal. The first term in Eq. (1), which we call $I_B(\mathbf{Q})$, is only non-zero at the Bragg points of the reciprocal lattice, and represents the modified Bragg peak intensities. The modifier, $d_n(\mathbf{Q})$, is commonly written as $e^{-W(\mathbf{Q})}$ and referred to as the "displacement" factor or the Debye-Waller (DW) factor. The displacement factor is often used to represent thermal disorder,[34] though it can clearly contain information about other types of defects and disorder. It modifies the diffracted intensities so as to correspond to the new average structure, which has been averaged over any distribution of local displacements. The second term in Eq.(1), which we refer to as $I_D(\mathbf{Q})$, is the diffuse scattering function, and is defined continuously over reciprocal space, rather than discretely. The diffuse scattering term directly probes the atomic displacement-displacement correlation function, which views the local displacements relative to one another rather than individually.[35] Thus, there is information about the nature of the local structure encoded in both the diffuse scattering the Bragg-diffracted intensities.

Static displacements produce only elastic scattering, whereas dynamic displacements either yield scattering features that have a finite quasi-elastic energy width that is inversely proportional to the time scale of the dynamics, or inelastic (phonon) scattering. X-ray scattering measurements typically integrate over a wide range of energies, and therefore produce a "snapshot" of the instantaneous displacements (i.e. broad energy resolution = narrow time range). Neutron scattering measurements, on the other hand, are commonly able to resolve the quasi-elastic width and/or inelastic response, allowing one to study the low-energy dynamics.

Total scattering experiments measure the average and local structure simultaneously, including quasi-elastic structure when it can be resolved. Single-crystal diffuse scattering is a particularly powerful tool because it measures full three-dimensional total scattering data. Some of its more challenging aspects include (1) the tremendous dynamic range required to simultaneously measure Bragg reflections and diffuse features in 3D reciprocal space without saturation, distortion, or loss of weak signals, (2) the collection, reconstruction, and reduction of 3D reciprocal space data from multi-detector hypersurfaces such that the end product is suitable for quantitative analysis, and (3) the computational burden of manipulating complex correlation models and large 3D scattering data sets. While valuable orientational information is lost in 1D scattering data from powder samples, the problems of dynamic range, data reduction, and computer power are much less severe for powder methods. Atomic pair distribution function (PDF) analysis, applied to powder samples, is a total scattering method in which powder diffraction data are Fourier-transformed to real-space coordinates[36] before being analyzed using techniques analogous to Rietveld refinement.[37] Rietveld analysis accesses the average local displacements via the DW factor, whereas the PDF method includes the diffuse-scattering intensity, $I_D(Q)$, thereby providing the potential to study locally correlated displacements.

The analytical tools that have been applied to the study of both average structure and local structure problems [38] tend to be classified according to three common denominators (1) a multi-parameter structural model, (2) an algorithm for navigating the multi-parameter space, and (3) an agreement-factor defined over the parameter space. An effective algorithm is tailored to the application at hand and should be thorough (samples all of the relevant parameter space), efficient (moves quickly towards good solutions), and robust (escapes local minima). A well-designed agreement factor will effectively differentiate a parameter set that approximates the true structure from one that does not over a wide dynamic range of "agreement", and should be sensitive to the model selected. The common use of a least-squares or steepest-descent algorithm, together with an agreement factor that measures only the difference between experimental and calculated data (e.g. diffraction or PDF data), might be termed the "straightforward" approach. However, the choice of model, algorithm, and agreement-factor is bounded only by the imagination. The Monte Carlo algorithm, for example, can be used in conjunction with agreement factors based purely on inter-atomic potentials as well as agreement factors based on a fit to experimental diffuse scattering data.[38] As data collection, reduction, and analysis tools improve, we move steadily towards the ability to apply a suite of fully three-dimensional PDF ("3DPDF") tools to single-crystal total scattering data.

IV. POLARONS FROM POWDERS

Long-range C/O-order is typically observed at special compositions with simple fractional values of x. In $LaSr_2Mn_2O_7$ (x = 0.5), for example, the resistivity rises sharply at T_{CO}, but falls off again as the C/O state gives way to a competing magnetic structure consisting of AF-coupled ferromagnetic sheets.[25] Most manganites that exhibit large CMR effects, however, do not exhibit long-range C/O order, despite their strongly analogous physical behavior. The resistivity of $La_{1.2}Sr_{1.8}Mn_2O_7$ (x = 0.4) increases rapidly with decreasing temperature despite the absence of a C/O-ordered state and drops precipitously at $T_C \sim 120$ K to make way for an entirely ferromagnetic structure.[39] The state above T_C is clearly polaronic, but very difficult to characterize structurally since the polaronic structure is local rather than crystalline.

Much of our knowledge of polaronic structure has been obtained from scattering experiments on polycrystalline samples. In $La_{1-x}Ca_xMnO_3$, the neutron powder PDF peak near 1.95Å corresponds to the Mn-O bond. At x = 0, this peak is split due to the presence of JT distortions[40,41], so that separate peaks appear at 1.92 Å and 2.12 Å. Because the splitting also occurs in the crystallographic-model PDF, it is clear that these are the cooperative or "coherent" JT distortions of the average structure. At x = 0.25, however, the PDF peak associated with the JT-elongated bond appears above T_C, even in the absence of any coherent JT distortions in the crystallographic average structure, implying the presence of local "incoherent", and possibly dynamic, distortions.[42] Note the exceptional quality of the fit to the crystallographic model below T_C in Fig. 4, and the significant discrepancies between the crystallographic and data PDFs above T_C. The Mn-O bond distortions disappear below T_C, where the e_g electrons become delocalized, demonstrating that the observed distortions are polaronic in origin.

The PDF peak at 2.75 Å corresponding to O-O bonds is also a sensitive probe of polaronic local structure. While the integrated area of this peak is independent of temperature, it is observed to markedly broaden below T_C at x = 0.21 and x = 0.25, which causes the peak height to decrease. The evolution of the 2.75 Å peak height vs. temperature appears in Fig. 5. Below T_C, the peak is sharp, indicating a resolution-

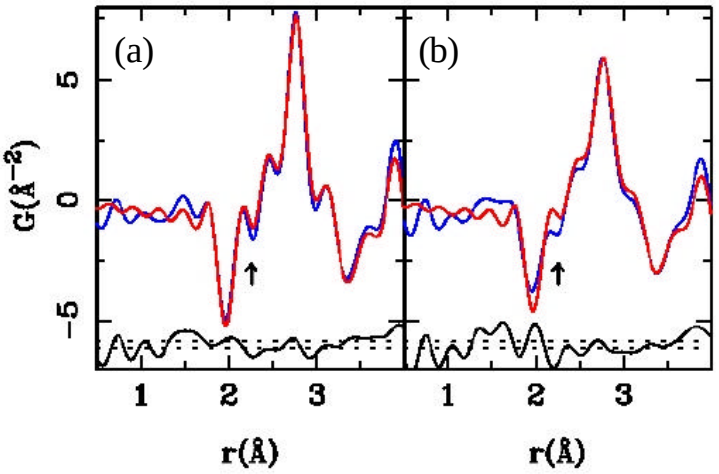

Figure 4. Best fit of the crystallographic model to neutron-powder PDF data for $La_{1-x}Ca_xMnO_3$ at x = 0.25 both below and near T_C. a) 10 K and b) 220K. The darker line is the data PDF, while the lighter line represents the model PDF. The difference PDF appears at the bottom of the figure, where straight dashed lines indicate the 2σ uncertainty level due to counting statistics. After Billinge.[14]

limited O-O bond-length distribution and providing further evidence that the polarons vanish in the FM state. This evidence is corroborated by XAFS results from a series of samples from x = 0 to 1 which show a pronounced anomalous broadening of the Mn-O bond length distribution above T_C for compositions with a FM ground state.[43] The DW factors also contain evidence of local polaronic distortions. In $La_{1-x}Ca_xMnO_3$ (x = 0.21 and 0.33) and $La_{1-x}Pb_xMnO_3$ (x = 0.30), the isotropic oxygen DW parameters obtained from Rietveld refinements are seen to clearly drop below T_C, accompanied by a slight decrease in the lattice parameters (see Fig. 6).[44,45] This again reflects the disappearance of local JT distortions in the FM state and the concomitant decrease in the disorder at the oxygen sites. A similar but weaker effect is also seen in the DW parameters of the A and B-site cations.[45]

The early PDF data from $La_{0.79}Ca_{0.21}MnO_3$ provided a remarkably detailed picuture of polaronic distortions in the insulating state above T_C. At these doping levels (x < 0.5) the charge carriers are hole-type Mn^{4+} polarons in an electron-rich Mn^{3+} matrix. Efforts to model the PDF data revealed the presence of small isotropic MnO_6 octahedra (associated with Mn^{4+} sites) coexisting with elongated JT-distorted ones (associated with Mn^{3+} sites), such that the long and short bond lengths differed by about 0.24 Å,[42] which is similar to the difference observed in orbitally-ordered $LaMnO_3$.[15] The octahedra occupied by hole-type polarons were observed to be uniformly contracted ($\delta \sim 0.12$) compared to the average structure. The PDF model, for the sake of convenience only, consisted of a particular C/O-ordering scheme similar to that of Fig. 3, but modified for a doping level of x=0.25, with every second Mn^{4+} site replaced by a Mn^{3+} site with its long JT-distorted Mn-O bond oriented out of the plane.[46] While these details were only explained in the later work[46], the excellent fit to the early PDF data[42] well beyond 10 Å suggested that this C/O ordering scheme had merit. As discussed below, subsequent

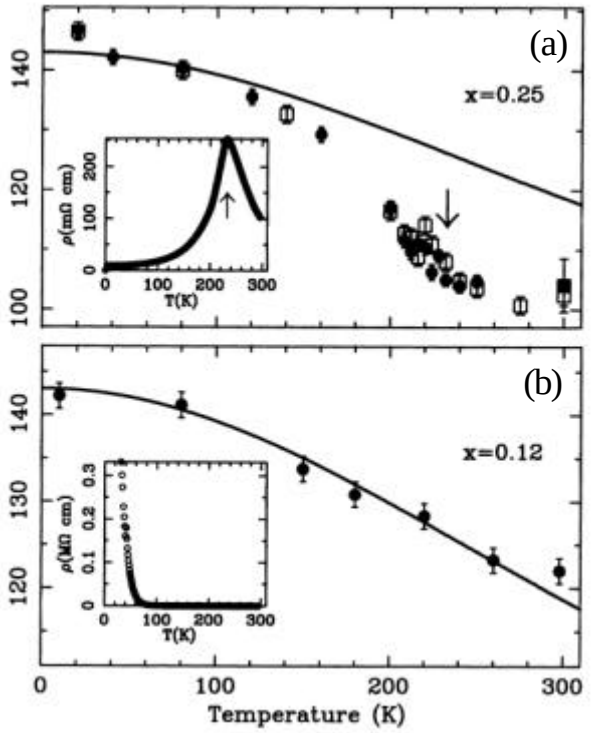

Figure 5. The neutron-powder PDF peak-height (2.75 Å) vs temperature for $La_{1-x}Ca_xMnO_3$ at a) x = 0.25 and b) x = 0.12. At x = 0.25, this peak, which is located at the nearest-neighbor O-O separation distance, anomalously broadens and falls-off above T_C (indicated by arrows). In contrast, the smooth variation of the peak shape at x = 0.12 is consistent with ordinary thermal vibrations. Circles and squares are data collected on cooling and warming, respectively. Corresponding resistivity data appear in the insets. After Billinge *et al.*[42]

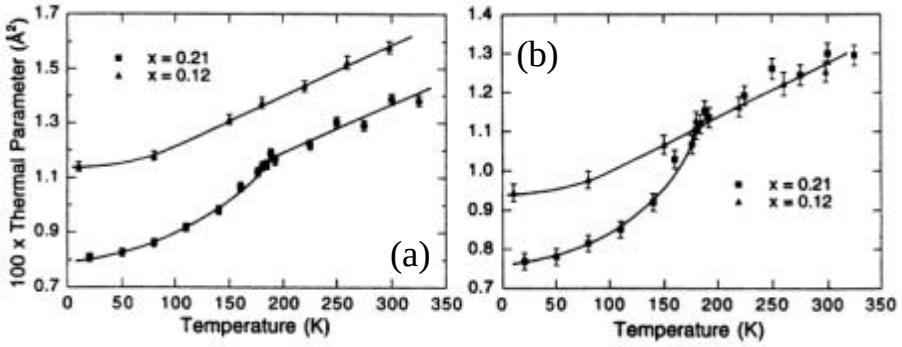

Figure 6. Temperature dependence of the isotropic Debye-Waller factors of the a) planar and b) apical oxygens of $La_{1-x}Ca_xMnO_3$ (x = 0.12 and x = 0.21) from neutron powder diffraction data. Note the anomalous increase observed upwards above T_C. After Kwei *et al.*[45]

single crystal diffuse scattering measurements conclusively demonstrated that short-range CE-type polaron correlations do occur in $La_{1-x}Ca_xMnO_3$ and other related systems.

Powder diffraction studies of $La_{1+2x}Sr_{2-2x}Mn_2O_7$ have shown that as the doping level is varied from x = 0.32 to x = 0.40, there is an unusual structural crossover effect in the coherent octahedral distortion amplitude at the optimum doping level, x_{opt} = 0.36.[47,48,49] This is explained in terms of distorted $Mn^{3+}O_6$ octahedra that shrink and $Mn^{4+}O_6$ octahedra that expand when the e_g electrons are delocalized, as in the case of the PDF results[42] from $La_{0.79}Ca_{0.21}MnO_3$. Most importantly, the oxygen DW factors of $La_{1+2x}Sr_{2-2x}Mn_2O_7$ reveal that the amplitude of the incoherent JT distortions is completely disconnected from that of the average coherent JT distortion. Independent of x, these local distortions build up above T_C and vanish abruptly at T_C, demonstrating that the polarons still collapse in the FM state.[48,50]

V. THE RISE AND FALL OF THE POLARON: STRAIN FIELDS AND DIFFUSE SCATTERING

The most detailed information about the three-dimensional structure of JT polarons in the CMR manganites comes from single crystal diffuse scattering (SCDS) experiments. X-ray and neutron SCDS, which has been used to study defects and disorder in a variety of materials[38] ranging from C_{60} to the high-T_C superconducting oxides[51], is also a powerful probe of the correlated displacements at the core of a JT distortion and the cooperative pattern of displacements that comprise any polaron-induced lattice strain fields that develop in response to the core displacements. Due to the nature of the Fourier transform, the sizes of related real and reciprocal space features are inversely related. Diffusely scattered features associated with displacements near the core of a distortion are broadly distributed across reciprocal space, whereas the diffuse scattering due to long-range strain-field displacements far from the core is distributed very close to the Bragg reflections. Obviously, because it is more localized in reciprocal space, the strain-field or "Huang" scattering[52] near a Bragg reflection is easier to measure. However, the core displacements are closely related to the strain-fields, and the physics that couples them is well understood.[35,53] Thus the diffuse strain-field scattering can be also used to obtain both local and extended polaronic structure.

Synchrotron x-ray diffuse scattering data have recently been obtained from single-crystal samples of several CMR perovskites that reveal unmistakable evidence of anisotropic strain-field scattering from polaronic lattice distortions.[54,55,56] Figure 7a contains a two-dimensional $(h0l)$ section of reciprocal space that includes the (0,0,8), (0,0,10), and (0,0,12) Bragg reflections of $La_{1.2}Sr_{1.8}Mn_2O_7$.[54] This scattering falls off like $1/q^2$ away from the allowed Bragg reflections, indicative of the typical long-range $1/r^2$ decay of the lattice strain fields away from point defect cores. And in addition to being proportional to the Bragg-peak structure factor, the strain-field scattering tends to be stronger for a Bragg peak far from the origin due to a factor of Q^2. The rod of scattering parallel to (0,0,1) centered at h = 0 is due to a low concentration of intergrowths of other members of the related Ruddlesden-Popper series: $(La/Sr)_{n+1}Mn_nO_{3n+1}$, and is unrelated to the polaron scattering. The "butterfly"-shaped anisotropy visible in Fig. 7a contains vital information about the symmetry and orientation of the JT distortions, relative to the perovskite bilayers. Fig. 7b, contains an $(h,k,0)$ section centered at (0,0,10.2), and reveals a three-dimensional scattering pattern that looks more like an hourglass than a butterfly, suggesting a distortion that is symmetric under 90° rotations (e.g. a $d(3x^2-r^2)$ type distortion). The weak anisotropy apparent at the edges of the figure is actually the result

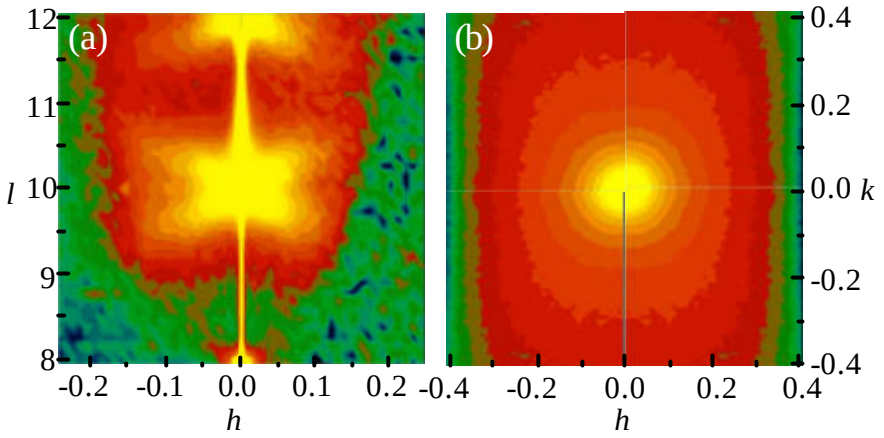

Figure 7. Contour plot showing the measured distribution of x-ray SCDS around the (0,0,10) reflection in $La_{1.2}Sr_{1.8}Mn_2O_7$ at 125 K. Panels (a) and (b) contain the (h,0,l) and (h,k,10.2) sections, respectively. After Vasiliu-Doloc *et al*.[54]

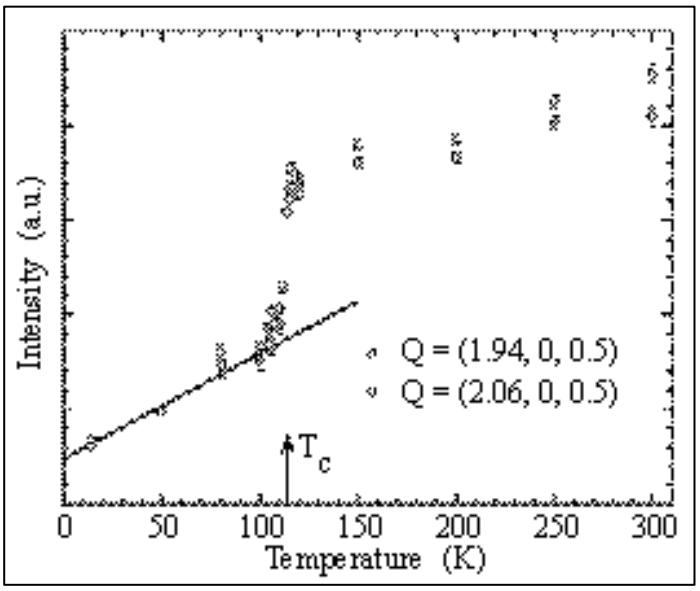

Figure 8. X-ray SCDS data from $La_{1.2}Sr_{1.8}Mn_2O_7$. Temperature dependence of the strain-field scattering measured on the two $l > 0$ lobes at $\mathbf{Q} = (2 \pm 0.06, 0, 0.5)$. The straight line indicates the contribution due to thermal diffuse scattering. The remainder of the scattering is associated with polaronic strain fields, which disappear abruptly below T_C, and get slowly damped out at high temperatures ($T >> 300$ K). After Vasiliu-Doloc *et al*.[54]

of x-ray absorption and the specific geometry of the sample. It should be noted, however, that these data are also qualitatively consistent with an average over $d(3x^2-r^2)$ and $d(3y^2-r^2)$ distortions. Complete three-dimensional SCDS data from a general Bragg position will resolve the true orbital character of these polarons.

In order to interpret the strain-field component of the x-ray diffuse scattering in Fig. 7, one must also take into account the contribution from thermal diffuse scattering (TDS), which arises from the instantaneous atomic displacements associated with thermally populated phonon modes. While the TDS also falls off as $1/q^2$ near allowed Bragg reflections, it can be confidently differentiated from the strain-field scattering via it's characteristic linear temperature dependence.[34] In Fig. 8a, the TDS contribution to the low-temperature butterfly scattering at (2±0.06, 0, 0.5) has been fitted to a straight line. The anomalous loss of intensity at the ferromagnetic transition temperature reveals the remainder of the scattering to be polaronic in nature and marks the sudden collapse of the polaronic state at T_C. The application of a magnetic field above T_C is also seen to destroy the strain-field contribution as the system is pushed into the FM state, providing a strong confirmation of the polaron hypothesis.[54]

In order to calculate the expected strain-field scattering distribution, one must determine the pattern of lattice displacements that arises in response to forces exerted by the defect center upon a finite number of atoms near the core. These displacements (assumed to be small) can then be inserted into Eq (1). Because the displacement field is impossible to calculate in all but the simplest cases, it's Fourier transform is generally calculated instead. This is the well-known method of static-displacement waves.[35,57] Finally, for scattering very near to the Bragg peak, we can employ the elastic approximation, which effectively embeds the details of a realistic JT polaron into an elastic continuum matrix. While there are many ways to group the various terms of the expression, we find it convenient to write the scattered intensity as:

$$I_{strain}(\mathbf{Q}) \propto |F_G|^2 Q_b Q_d T_{ag} D_{abgd} \quad , \text{ where} \tag{5}$$

$$T_{ag}(\mathbf{q}) = \sum_{\mathbf{R}_1,\mathbf{R}_2} \Im_a(\mathbf{R}_1)\Im_g(\mathbf{R}_2) e^{i\mathbf{q}\cdot(\mathbf{R}_1-\mathbf{R}_2)} \quad \text{and} \tag{6}$$

$$D_{abgd}(\mathbf{q}) = \sum_{j_1,j_2} \frac{\hat{e}_a(\mathbf{q},j_1)\hat{e}_b^*(\mathbf{q},j_1)\hat{e}_g^*(\mathbf{q},j_2)\hat{e}_d(\mathbf{q},j_2)}{w(\mathbf{q},j_1)^2 w(\mathbf{q},j_2)^2} \tag{7}$$

Here, $\mathbf{R}$ is an atomic position vector relative to the defect center, Á($\mathbf{R}$) is the force exerted by the defect core on the atom at $\mathbf{R}$, $\mathbf{q} = \mathbf{Q}-\mathbf{G}$ is a vector in the Brillouin zone corresponding to reciprocal lattice vector $\mathbf{G}$, $F_\mathbf{G}$ is the structure factor at $\mathbf{G}$, j is a phonon branch index, and $\omega_{\mathbf{q},j}$ and $\hat{\mathbf{e}}(\mathbf{q},j)$ are the eigen-frequencies and eigenvectors of the continuum dynamical matrix. The sums over Greek indices are implicit sums over vector and tensor components. To this, we add the TDS contribution, which may be written in the same notation as:

$$I_{TDS}(\mathbf{Q}) \propto |F_G|^2 Q_a Q_b \sum_j \frac{\hat{e}_a(\mathbf{q},j)\hat{e}_b^*(\mathbf{q},j)}{w(\mathbf{q},j)^2} \tag{8}$$

The calculated x-ray SCDS pattern around the (0,0,10) Bragg reflection that appears in Fig. 9 employs reasonable values of the tetragonal elastic constants to obtain the dynamical matrix, and assumes that forces are applied only to the six oxygens of the

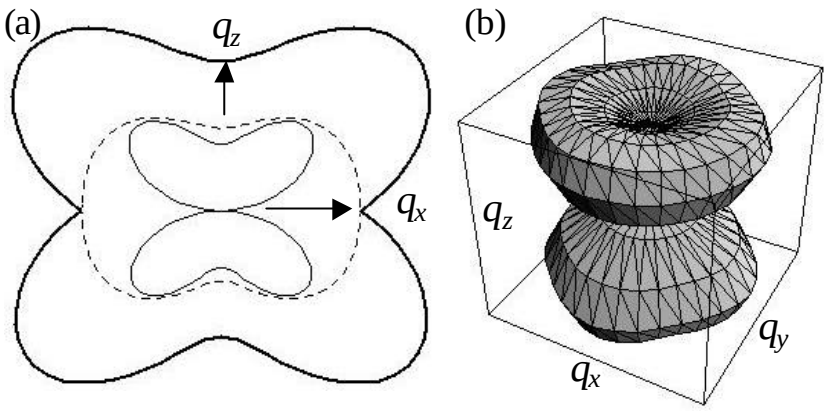

Figure 9. Calculated x-ray SCDS distribution around the (0,0,10) Bragg reflection of $La_{1.2}Sr_{1.8}Mn_2O_7$, based on a local JT stretch || (001) in an elastic medium. (a) Calculated iso-intensity contours for the strain-field scattering (thin solid line) and TDS (dashed line) contributions to the total scattering (thick solid line) in the (*h*,0,*l*) plane. (b) Calculated iso-intensity surface of the three-dimensional strain-field scattering distribution.

MnO_6 unit that defines the distortion core. Fig. 9b illustrates the relative contributions of the strain-field scattering and TDS to the overall scattering pattern. Note that the strain-field scattering possesses well-defined lobes, whereas the anisotropy of the TDS is more subtle. This fact makes interpreting the x-ray SCDS patterns somewhat easier.

VI. POLARON CORRELATIONS AT THE NANOSCALE

Weak diffuse satellite reflections were recently reported to appear in x-ray SCDS data from $La_{1.2}Sr_{1.8}Mn_2O_7$, indicating the presence of nanoscale spatial polaron correlations above T_C.[54] Fig. 10 contains single-crystal x-ray and neutron diffuse scattering data from this layered system[58] that simultaneously reveals anisotropic strain-field scattering from uncorrelated polarons together with several polaron-correlation peaks. Related features have since been discovered in a number other perovskite manganites[55,56,59,60], suggesting that short-range polaron correlations may be general participants in CMR phenomena.

In $La_{1-x}Ca_xMnO_3$, single-crystal neutron diffuse-scattering data reveal broad diffuse peaks at reciprocal-space positions that correspond to propagation vector **q** = (0.25, 0.25, 0) and appear to indicate a short-range incipient form of CE-type C/O order (see Fig. 11a).[59] Like the elastic strain-field scattering associated with uncorrelated polarons, the temperature dependence of the diffuse CE-C/O peaks builds up above T_C and drops sharply to zero at the FM transition. Because this transition is accompanied by a significant CMR effect, one might expect that it can be assisted via the application an external magnetic field. This is indeed the case[54,59], as illustrated in Fig. 11b. The ground state of $La_{0.8}Ca_{0.2}MnO_3$ (x = 20), on the other hand, is not metallic[44], and its polaron correlations persist below T_C.[60] This close relationship between the local structure and the macroscopic transport makes it clear that the charge carriers are polaronic.

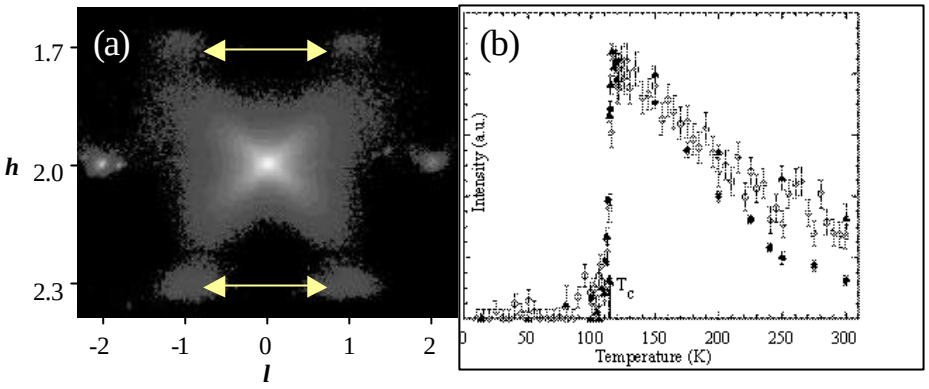

Figure 10. Single-crystal x-ray diffuse scattering data from $La_{1.2}Sr_{1.8}Mn_2O_7$. (a) CCD image of high-energy x-ray SCDS data from the (*h*,0.05,*l*) plane surrounding the (2,0,0) Bragg reflection (logarithmic scale). The diffuse butterfly-shaped scattering pattern is a combination of polaronic strain-field scattering and anisotropic thermal diffuse scattering, while the four diffuse maxima indicated by arrows are evidence of nanoscale polaron correlations. The peaks on the far left and right are tails of the (2,0,±2) Bragg reflections. After Campbell *et al.*[58] (b) Nearly identical trends of the polaron-correlation peak at **Q** = (2.3,0,1) [x-rays, closed circles] and the polaronic strain-field scattering at **Q** = (2±0.06,0,0.5) [x-rays, TDS corrected, closed triangles] and **Q** = (2.05,0,0.25) [quasi-elastic neutron scans, open circles]. After Vasiliu-Doloc *et al.*[54]

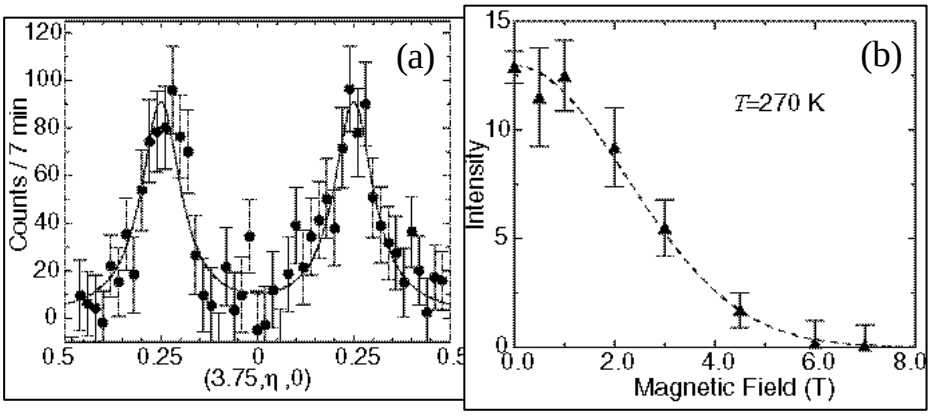

Figure 11. (a) Single-crystal neutron diffuse scattering from $La_{0.7}Ca_{0.3}MnO_3$. This (h,-h,0) scan through a pair of (3.75, 0.25, 0) peaks indicates a short-range analogue of CE-type charge/order. After Adams *et al.*[59] (b) The magnetic field dependence of the (3.75,0.25,0) polaron correlations peak at 270 K. After Lynn *et al.*[59]

At lower doping levels, the propagation vector associated with the short-range polaron correlations **q** = (0.25+ε, 0.25-ε, 0) becomes slightly incommensurate, much like that observed in the case of long-range C/O in $La_{0.5}Ca_{0.5}MnO_3$,[19] with a value of ε = 0.05 being reported[60] for $La_{0.8}Ca_{0.2}MnO_3$. When the doping level is reduced to x = 0.15, however, the diffuse peaks appeared at entirely different positions[60] which appear to be

consistent with the more complicated long-range C/O configuration reported for $La_{1-x}Sr_xMnO_4$ ($x \sim 0.125$).[61] $Pr_{0.7}Ca_{0.3}MnO_3$ provides an interesting combination of incommensurate long and short-range C/O order.[56] Here, critical charge and orbital fluctuations are evidenced by diffuse CE-C/O satellites with an incommensurability that decreases with temperature and finally locks in at $\varepsilon = 0$ when the correlation length diverges at $T_{CO} \sim 230$ K.

Like the C/O fluctuations, the ferromagnetic spin fluctuations in $La_{0.7}Ca_{0.3}MnO_3$ build up as T_C is approached from above.[59] Below T_C, the central quasi-elastic peak of the spin fluctuations then disappears as spin-wave peaks develop in their place.[62,63] The intrinsic *q*-space widths were simultaneously measured for both the polaron-correlation peaks and the ferromagnetic-fluctuation peaks. The comparable correlation lengths, ~10 Å and 16 Å, respectively, suggest that the quasi-elastic spin fluctuation should be thought of as the spin component of a magnetic polaron. Figure 12 shows the nearly identical trends of the CE-C/O peak at (3.75,0.25,0), the central peak of the magnetic fluctuation spectrum at (1.03,0,0), and the sample resistivity.[59] In light of the competition between C/O order and long-range magnetic order, this surprising connection between the magnetic and polaronic fluctuations above T_C deserves further examination.

While the temperature and magnetic field behaviors of the polaron correlation peaks in $La_{1.2}Sr_{1.8}Mn_2O_7$, relative to the transition to the FM state at T_C, are mirrored by the $La_{0.7}Ca_{0.3}MnO_3$ system, the unusual propagation vector, $q = (0.3, 0, \pm 1)$, of the polaron correlations in the bilayered $La_{1+2x}Sr_{2-2x}Mn_2O_7$ system immediately set them apart as distinct from the CE-type correlations of the 3D perovskite manganites.[54,58] Though 90° twin domains are represented in equal proportions, these diffuse satellite reflections point to a one-dimensional incommensurate modulation along the (100) axes of the tetragonal $I4/mmm$ lattice. A crystallographic analysis of the integrated intensities of over 100 of these diffuse satellites yields the novel longitudinal JT stretch mode[58] shown in Fig. 13, which shall be referred to hereafter as "L"-type.[64] This pattern of distortions points to a JT-coupled charge density wave fluctuation, the structure of which has no known long-range analogue. The real-space correlation lengths are roughly $\xi_{\parallel} \approx 23$Å, $\xi_{\perp} \approx 15$Å, and $\xi_c \approx 10$Å, and triple-axis energy scans demonstrate that the structure is static on a 1 ps time scale.[54] Straightforward strain considerations additionally suggest that further-than-nearest-neighbor interactions must be responsible, while the fact that this arrangement has only been observed in a layered system may be connected to Fermi-surface effects reported to exist in the FM state below T_C.[65]

The predominant feature in Fig. 13 is the JT stretch mode of the Mn-O bonds that lie along the direction of the modulation. The Mn-O bonds that lie along (001) at a given site are compressed when the corresponding bonds along (100) are stretched, and vice-versa. A pattern of octahedral tilts accompanies the alternating expansion and compression of the Mn-O bonds in a physically intuitive way. Because the modulation amplitudes of all of the seven unique atoms have the same phase, we are able to represent the displacement directions with the sinusoidal solid and dashed curves shown in the figure. These relative phases of these curves are dictated by the symmetry of the modulation and show how the displacements in one perovskite sheet are related to those in another. Notably, this symmetry stacks the JT-distorted octahedra of a single bilayer together along the (010) direction, giving the underlying charge density wave a striped character as well. It also sets the modulations in adjacent bilayers to be 180° out of phase.[58]

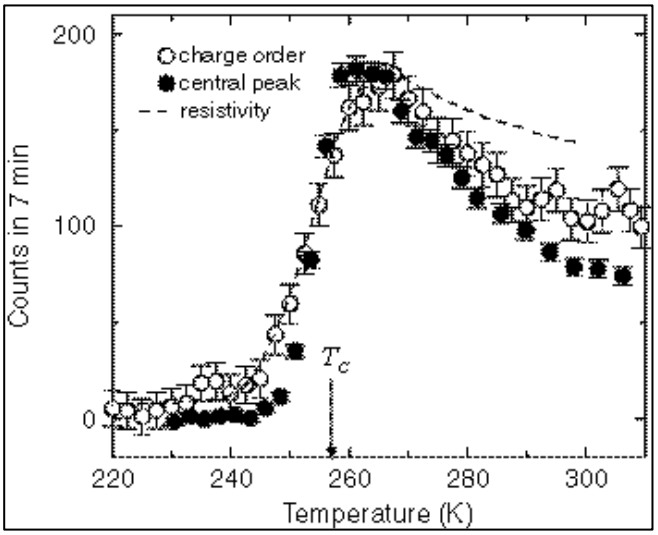

Figure 12. Single-crystal neutron diffuse scattering and transport data from $La_{0.7}Ca_{0.3}MnO_3$ reveals nearly identical temperature trends for the quasi-elastic magnetic fluctuation peak at (1.03,0,0), the polaron correlation peak at (3.75,0.25,0), and the bulk resistivity. After Adams *et al.*[59]

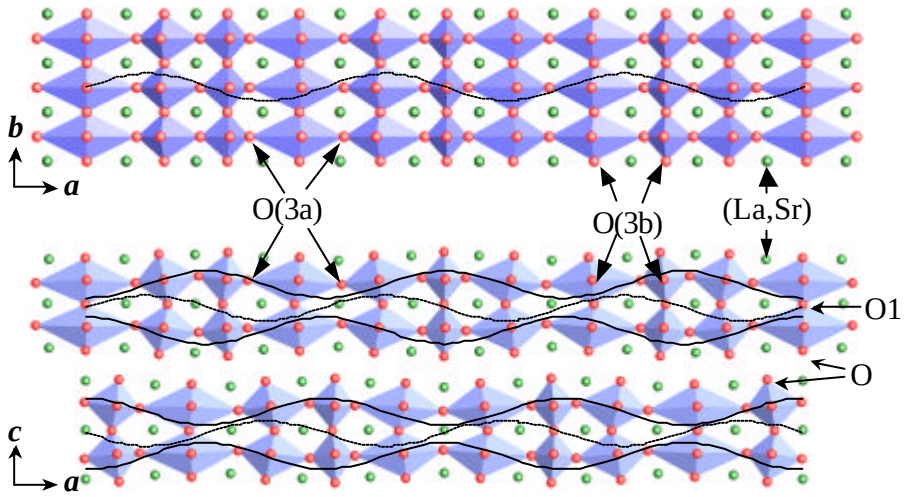

Figure 13. Crystallographic representation of the polaron correlations in $La_{1.2}Sr_{1.8}Mn_2O_7$. The directions of the atomic displacements within each perovskite sheet and bilayer follow the solid (*z*-component) and dashed (*x*-component) curves, where peaks indicate $+x$ or $+z$ displacements and troughs indicate $-x$ or $-z$ displacements. The displacements are exaggerated in order to make the more subtle features of the modulation visually apparent, and the modulation period has been approximated by the commensurate value of 10/3. After Campbell *et al.*[58]

VI. CONCLUDING REMARKS

The detailed crystallographic picture of coherent JT distortions, obtained in the limit of long-range C/O order, has added greatly to our understanding of CMR phenomena. The evolution of these coherent distortions and their associated superstructures at magnetic and metal-insulator transitions has firmly established a relationship between spin, charge, orbital, and lattice degrees of freedom at certain special compositions. Now, a growing suite of experimental and analytical scattering tools that are sensitive to local structural features have opened a new eye on the CMR universe. Local JT distortions have recently been observed to correlate strongly with anomalous magnetic and transport properties where no evidence of long-range C/O order could be found, demonstrating that the CMR effect in the perovskite manganites is derived from the existence of a polaronic state and its subsequent collapse under the influence of the double-exchange interaction.

Powder PDF and single-crystal diffuse scattering studies of JT polarons have uncovered a number of distinct structural features, including the local distortions of JT-distorted MnO_6 octahedra and the strain fields that comprise the accompanying lattice response. Furthermore, nanoscale (10 to 25 Å) polaron correlations have been discovered in several manganite systems, and can be viewed as a short-range form of C/O order that can exist over wide regions of the phase diagram that do not permit long-range order. Straightforward powder measurements quickly uncover features and trends of interest, while the more difficult and comprehensive single-crystal measurements are required to build a complete picture. Understanding this complementarity is important to the further development of both powder and single-crystal methods. Relevant issues that continue to intrigue us include the high-temperature fate of local JT-distortions and correlations, the time-scale of polaron dynamics, and the existence of local orientational order. Ongoing efforts to probe the local structure of the CMR manganites should address these and many other questions.

ACKNOWLEDGMENTS

Special thanks to a number of colleagues that have been involved in various aspects of this research, including C.P. Adams, D.N. Argyriou, A.A. Arsenov, A.R. Bishop, C. Booth, J.A. Borchers, E. Bozin, D.C. Dender, R.G. DiFrancesco, T. Egami, R.W. Erwin, A.J. Fedro, K. Ghosh, R.L. Greene, Q. Huang, M.F. Hundley, Z. Islam, S. Krasnicki, G.H. Kwei, Z.Y. Li, C.D. Ling, D. Louca, J.F. Mitchell, Y.M. Mukovskii, J.J. Neumeier, J.L. Peng, V. Petkov, G. Preosti, Th. Proffen, S. Rosenkranz, U. Ruett, A. Santoro, O. Seeck, D.A. Shulyatev, V.N. Smolyaninova, J.D. Thompson, M.F. Thorpe, L. Vasiliu-Doloc, and D. Vermeille. Research at ANL is supported by the U.S. Dept. of Energy, Office of Science under Contract No. W-31-109-ENG-38. Research at UM is supported by the NSF-MRSEC, DMR 00-80008. Research at MSU is supported by NSF grant DMR-0075149. Research at the Manuel Lujan Neutron Scattering Center at LANL was supported by the U.S. Dept. of Energy under contract W-7405-ENG-36.

REFERENCES

[1] G.H. Jonker, J.H. van Santen, Physica **16**, 337 (1950).
[2] R.M. Kusters, J. Singleton, D.A. Keen, R. McGreevy, W. Hayes, Physica B **155**, 362 (1989).
[3] J. Volger, Physica **20**, 49 (1954).
[4] C. Zener, Phys. Rev. **82**, 403 (1951).
[5] P.G. de Gennes, Phys. Rev. **118**, 141 (1960).
[6] A.J. Millis, P.B. Littlewood, B.I. Shraiman, Phys. Rev. Lett. **74**, 5144 (1995).
[7] H. Röder, J. Zang, A.R. Bishop, Phys. Rev. Lett. **76**, 1356 (1996).
[8] D. Emin, Mat. Res. Soc. Symp. Proc. **494**, 163 (1998).
[9] J. Tanaka, M. Umehara, S. Tamura, M. Tsukioka, S. Ehara, J. Phys. Soc. Jpn. **51**, 1236 (1982).
[10] H.A. Jahn, E. Teller, Proc. R. Soc. London A **161**, 220 (1937); J. H. van Vleck, J. Chem. Phys. **7**, 72 (1939).
[11] A. Moreo, S. Yunoki, E. Dagotta, Science **283**, 2034 (1999).
[12] J.B. Goodenough, Annu. Rev. Mater. Sci. **28**, 1 (1998).
[13] J.B. Goodenough, Phys. Rev. **100**, 564 (1955).
[14] See articles by Billinge, Tomioka *et al*., Noh *et al*., Zhao *et al.*, and Jaime *et al.*, in *Physics of Manganites*, eds. T.A. Kaplan and S.D. Mahanti, Kluwer Academic/Plenum Publishers, New York (1999).
[15] J.F. Mitchell, D.N. Argyriou, C.D. Potter, D.G. Hinks, J.D. Jorgensen, S.D. Bader, Phys. Rev. B **54**, 6172 (1996).
[16] J.B. Goodenough and J.M. Longo in *Landolt-Börnstein Tabellen*, New Series III/4a, pp. 126-314, ed. K.H. Hellwege, Springer-Verlag (1970).
[17] E.O. Wollan, W. C. Koehler, Phys. Rev. **100**, 545 (1955).
[18] C.H. Chen, S.-W. Cheong, Phys. Rev. Lett. **76**, 4042 (1996).
[19] P.G. Radaelli, D.E. Cox, M. Marezio, S.-W. Cheong, Phys. Rev. B **55**, 3015 (1997).
[20] Q. Huang, J.W. Lynn, R.W. Erwin, A. Santoro, D.C. Dender, V.N.Smolyaninova, K. Ghosh, R.L. Greene, Phys. Rev. B **61**, 8895 (2000).
[21] J.F. Mitchell, D.N. Argyriou, J.D. Jorgensen, in *Colossal Magnetoresistive Oxides*, ed. Y. Tokura, Gordon & Breach (2000).
[22] C.N.R. Rao, A. Arulraj, A.K. Cheetham, B. Raveau, J. Phys. Cond. Mater. **12**, R83 (2000).
[23] S. Mori, C.H. Chen, S.-W. Cheong, Nature **392**, 473 (1998).
[24] P.G. Radaelli, D.E. Cox, L. Capogna, S.-W. Cheong, M. Marezio, Phys. Rev. B **59**, 14440 (1999).
[25] D.N. Argyriou, H.N. Bordallo, B.J. Campbell, A.K. Cheetham, D.E. Cox, J.S. Gardner, K. Hanif, A. dos Santos, G.F. Strouse, Phys. Rev. B **61**, 15269 (2000).
[26] T. Kimura, R. Kimai, Y. Tokura, J.Q. Li, Y. Matsui, Phys. Rev. B **58**, 11081 (1998).
[27] M. Kubota, K. Yoshizawa, Y. Moritomo, H. Fujioka, K. Hirota, Y. Endoh, J. Phys. Soc. Jpn. **68**, 2202 (1999).
[28] Z. Jirak, S. Krupicka, Z. Simsa, M. Dlouha, S. Vratislav, J. Magn. Magn. Mater. **53**, 153 (1985).
[29] H. Yoshizawa, H. Kawano, Y. Tomioka, Y. Tokura, Phys. Rev. B **52**, 13145 (1995).
[30] Y. Tomioka, A. Asamitsu, Y. Moritomo, Y. Tokura, J. Phys. Soc. Jpn. **64**, 3626 (1995).
[31] V. Kiryukin, D. Casa, J.P. Hill, B. Keimer, A. Vigliante, Y. Tomioka, Y. Tokura, Nature **386**, 813 (1997).
[32] M.v. Zimmerman, J.P. Hill, D. Gibbs, M. Blume, D. Casa, B. Keimer, Y. Murakami, Y. Tomioka, Y. Tokura, Phys. Rev. Lett. **83**, 4872 (1998).

[33] Y. Murakami, H. Kawada, M. Tanaka, T. Arima, Y. Moritomo, Y. Tokura, Phys. Rev. Lett. **80**, 1932 (1998).
[34] B.T.M. Willis, A.W. Pryor, *Thermal Vibrations in Crystallography*, Cambridge Univ. Press, Cambridge (1975).
[35] M.A. Krivoglaz, *X-ray and neutron diffraction in non-ideal crystals*, Eng. translation, Springer-Verlag, Berlin/Heidelberg (1996).
[36] See articles by T. Egami and S.J.L. Billinge, in *Local Structure from Diffraction*, eds. S.J.L. Billinge and M.F. Thorpe, Plenum Publishers, New York (1998).
[37] R.A. Young, in *The Rietveld Method*, ed. R.A. Young, IUCr Monograph No. 5, Oxford Univ. Press (1993).
[38] See articles and accompanying references in *Local Structure from Diffraction*, eds. S.J.L. Billinge and M.F. Thorpe, Plenum Publishers, New York (1998).
[39] Y. Moritomo, A. Asamitsu, H. Kuwahara, Y. Tokura, Nature **380**, 141 (1996).
[40] Th. Proffen, R.G. DiFrancesco, S.J.L. Billinge, E.L. Brosha, G.H. Kwei, Phys. Rev. B **60**, 9973 (1999).
[41] D. Louca, G.H. Kwei, J.F. Mitchell, Phys. Rev. Lett. **80**, 3811 (1998).
[42] S.J.L. Billinge, R.G. DiFrancesco, G.H. Kwei, J.J. Neumeier, J.D. Thompson, Phys. Rev. Lett. **77**, 715 (1996).
[43] C.H. Booth, F. Bridges, G.H. Kwei, J.M. Lawrence, A.L. Cornelius, J.J. Neumeier, Phys. Rev. Lett. **80**, 853 (1998).
[44] Q. Huang, A. Santoro, J.W. Lynn, R.W. Erwin, J.A. Borchers, J.L. Peng, K. Ghosh, R.L. Greene, Phys. Rev. B **58**, 2684 (1998).
[45] G.H. Kwei, D.N. Argyriou, S.J.L. Billinge, A.C. Lawson, J.J. Neumeier, A.P. Ramirez, M.A. Subramanian, J.D. Thompson, Mat. Res. Soc. Symp. Proc. **475**, 533 (1997).
[46] S.J.L. Billinge, Th. Proffen, V. Petkov, J.L. Sarrao, S. Kycia, Phys. Rev. **62**, 1203 (2000).
[47] J.F. Mitchell, D.N. Argyriou, J.D. Jorgensen, D.G. Hinks, C.D. Potter, S.D. Bader, Phys. Rev. B **55**, 63 (1997).
[48] M. Medarde, J.F. Mitchell, J.E. Milburn, S. Short, J.D. Jorgensen, Phys. Rev. Lett **83**, 1223 (1999).
[49] D.N. Argyriou, H.N. Bordallo, J.F. Mitchell, J.D. Jorgensen, G.F. Strouse, Phys. Rev. B **60**, 6200 (1999).
[50] The term "collapse" here refers to the disappearance of the JT polaron, whereas in Ref. [8], it is used to describe small polaron formation.
[51] S.T. Johnson, P.D. Hatton, A.J.S. Chowdhury, B.M. Wanklyn, Y.F. Yan, Z.X. Zhao, A. Marshall, Physica C **219**, 61 (1994).
[52] K. Huang, Proc. Royal Soc. A **190**, 102 (1947).
[53] P.H. Dedhrichs, J. Phys. F Metals Phys. **3**, 471 (1973).
[54] L. Vasiliu-Doloc, S. Rosenkranz, R. Osborn, S.K. Sinha, J.W. Lynn, J. Mesot, O.H. Seeck, G. Preosti, A.J. Fedro, J.F. Mitchell, Phys. Rev. Lett. **83**, 4393 (1999).
[55] S. Shimomura, N. Wakabayashi, H. Kuwahara, Y. Tokura, Phys. Rev. Lett. **83**, 4389 (1999).
[56] S. Shimomura, T. Tonegawa, K. Tajima, N. Wakabayashi, N. Ikeda, T. Shobu, Y. Noda, Y. Tomioka, Y. Tokura, Phys. Rev. B **62**, 3875 (2000).
[57] For a detailed presentation of the phonon formulation, see A.A. Maradudin, E.W. Montroll, G.H. Weiss, I.P. Ipatova, Theory of Lattice Dynamics in the Harmonic Approximation, 2nd ed., Academic Press, New York (1971).

[58] B.J. Campbell, R. Osborn, D.N. Argyriou, L. Vasiliu-Doloc, J.F. Mitchell, S.K. Sinha, U. Ruett, C.D. Ling, Z. Islam, J.W. Lynn, Phys. Rev. B, *in press*, cond-mat/0106577 (2001).
[59] C.P. Adams, J.W. Lynn, Y.M. Mukovskii, A.A. Arsenov, D.A. Shulyatev, Phys. Rev. Lett. **85**, 3954 (2000); J.W. Lynn, C.P. Adams, Y.M. Mukovskii, A.A. Arsenov, D.A. Shulyatev, J. Appl. Phys. **89**, 6846 (2001).
[60] P.-C. Dai, J.A. Fernandez-Baca, N. Wakabayashi, E.W. Plummer, Y. Tokura, Phys. Rev. Lett. **85**, 2553 (2000).
[61] Y. Yamada, O. Hino, S. Nohdo, R. Kanao, T. Inami, S. Katano, Phys. Rev. Lett. **77**, 904 (1996).
[62] J. W. Lynn, R. W. Erwin, J. A. Borchers, Q. Huang, A. Santoro, J. L. Peng, and Z. Y. Li, Phys. Rev. Lett. **76**, 4046 (1996); J. W. Lynn, R. W. Erwin, J. A. Borchers, A. Santoro, Q. Huang, J. L. Peng and R. L. Greene, J. Appl. Phys. **81**, 5488 (1997).
[63] For a recent review of the spin dynamics see J. W. Lynn, J. Superconductivity and Novel Magnetism **13**, 263 (2000).
[64] This label was suggested by D.N. Argyriou.
[65] Y.-D. Chuang, A.D. Gromko, D.S. Dessau, T. Kimura, Y. Tokura, Science **292**, 1509 (2001).